fluids

MDPI

Article

The Effect of Bifurcated Geometry on the Diodicity of Tesla Valves

Sean Wiley * and **Huei-Ping Huang**

School for Engineering of Matter, Transport, and Energy, Arizona State University, Tempe, AZ 85281, USA; hp.huang@asu.edu
* Correspondence: spwiley@asu.edu

Abstract: The Tesla valve is a fluidic diode that enables unidirectional flow while impeding the reverse flow without the assistance of any moving parts. Conventional Tesla valves share a distinctive feature of a bifurcated section that connects the inlet and outlet. This study uses computational fluid dynamic (CFD) simulations to analyze the importance of the bifurcated design to the efficiency of the Tesla valve, quantified by *diodicity*. Simulations over the range of the Reynolds number, Re = 50–2000, are performed for three designs: the T45-R, D-valve, and GMF valve, each with two versions with and without the bifurcated section. For the T45-R valve, removing the bifurcated section leads to a consistent increase in diodicity, particularly at high Re. In contrast, the diodicity of the GMF valve drops significantly when the bifurcated section is removed. The D-valve exhibits a mixed behavior. Without the bifurcated section, its diodicity is suppressed at low Re but begins to increase for $Re > 1100$, eventually matching the diodicity of the bifurcated version at $Re = 2000$. The results highlight the intricate relationship between valve geometry and efficiency of Tesla-type valves and the dependence of this relationship on the Reynolds number.

Keywords: Tesla valve; fluidic diode; flow control

check for updates

Citation: Wiley, S.; Huang, H.-P. The Effect of Bifurcated Geometry on the Diodicity of Tesla Valves. *Fluids* **2024**, *9*, 294. https://doi.org/10.3390/fluids9120294

Academic Editors: Robert Martinuzzi and Michele Ferlauto

Received: 6 November 2024
Revised: 8 December 2024
Accepted: 10 December 2024
Published: 11 December 2024

1. Introduction

In fluid mechanics, the Tesla valve presents an intriguing avenue for addressing fluid control challenges. Nikola Tesla patented his "valvular conduit" in 1920 [1], which created a method to non-mechanically restrict fluid flow to one direction. The non-mechanical valve became known as the Tesla valve, which has recently undergone a revival (Begg [2]) in new applications for microfluidic systems (e.g., Li et al. [3], Raffel et al. [4], Wang et al. [5], Zhang et al. [6]) and novel devices for heat transfer (e.g., Li et al. [3], de Vries et al. [7], Monika et al. [8], Gajjar and Huang [9]). Tesla's design, illustrated in Figure 1, effectively was a fluidic diode. Due to asymmetry in the geometry, to maintain the same flow rate, the required pressure drop in the reverse direction (ΔP_r) exceeds that in the forward direction (ΔP_f). The ratio of the two is defined as *diodicity*, Di,

$$Di = \Delta P_r / \Delta P_f. \tag{1}$$

A diodicity greater than 1 indicates a promotion of the flow in the forward direction. The diodicity of a Tesla valve varies with the Reynolds number, Re. At very small Re, the diodic behavior diminishes such that $Di \approx 1$. At a low Reynolds number up to $Re \approx 500$, Di is known to increase monotonically with Re for several designs of the Tesla valve (Raffel et al. [4], de Vries et al. [7], Forster et al. [10], Thompson et al. [11]). For example, Di reaches 1.2 at $Re = 300$ for the T45-R valve, based on a 3D CFD simulation and experimental data (Thompson et al. [11]). The behavior of diodicity at a higher Reynolds number has not been extensively explored, but Zhang et al. [6] showed a continued increase of Di with Re up to $Re = 2000$ for the T45-R valve. Many applications adopt a multi-staged setting by connecting several Tesla valves in a chain (cf. Figure 1). This helps enhance diodicity, although the enhancement does not scale linearly with N, the number of valves in the chain. Thompson et al. [11] showed an example in which Di increases from 1.5 at N = 1 (single valve) to a saturated value of 1.8 at N = 8, beyond which adding more valves to the chain does not help increasing Di further. In this study, for conciseness, we will focus on the case with N = 1.

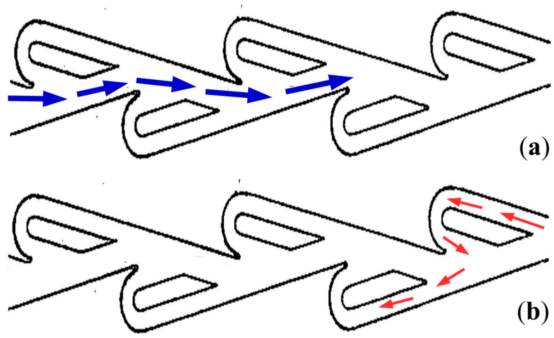

Figure 1. Multi-staged classical Tesla valve and an illustration of the asymmetry between two directions: (**a**) Forward flow; (**b**) Reverse flow.

The Tesla valves used in modern applications differ in detail from the original sketch by N. Tesla. Figure 2 shows three examples of newer designs which will be investigated in this work. (a) *T45-R valve*, after Forster at al. [10] and Thompson et al. [11]. Forster et al. [10] designed it for flow control in a piezoactuated pump, demonstrating that its efficiency exceeds that of conventional diffuser check valves. The name reflects the 45-degree angle between the inlet and outlet segments. (b) *D-valve*, after de Vries et al. [7], who designed it for applications to pulsating heat pipes. The valve consists of aligned inlet and outlet segments and highly curved branches. (c) *GMF valve*, after Gamboa et al. [12] and Thompson et al. [11]. It is modified from the T45-R valve with a more dramatic contrast between the two branches; the curved one is made longer and with a greater curvature. Further variations of the three designs in Figure 2 have been used in applications. For example, Wang et al. [13] modified the GMF valve by adding multiple bottlenecks along the pipe.

Despite the variations in detail, these modern designs and the original Tesla valve share common geometric characteristics of a single inlet and outlet, angled fluid flow, and a bifurcated section. This study explores alternative designs that do not strictly adhere to these characteristics (particularly, the bifurcated geometry) yet still possess a diodic behavior. To motivate the study, we briefly survey how the classical Tesla valve works (e.g., Raffel et al. [4], Pattanshetti [14], Zeidan et al. [15]). The greater resistance in the reverse direction is associated with the adverse pressure gradients from diverging sections that result in stagnation, flow reversal, and generation of vortices (see examples in Raffel et al. [4]). In a Tesla valve, the reverse flow may split into a primary and secondary flow, and the secondary flow diverges and rejoins the primary flow at some angle. A vortex forms where the secondary flow joins and turns to the direction of the primary flow. The adverse pressure gradient in the secondary flow and the vortex creates notable energy losses that induce a pressure drop for the reverse flow, but minimal difference for the forward flow. Since flow separation and generation of vortices do not occur at a very low Reynolds number, the diodic behavior diminishes at that limit.

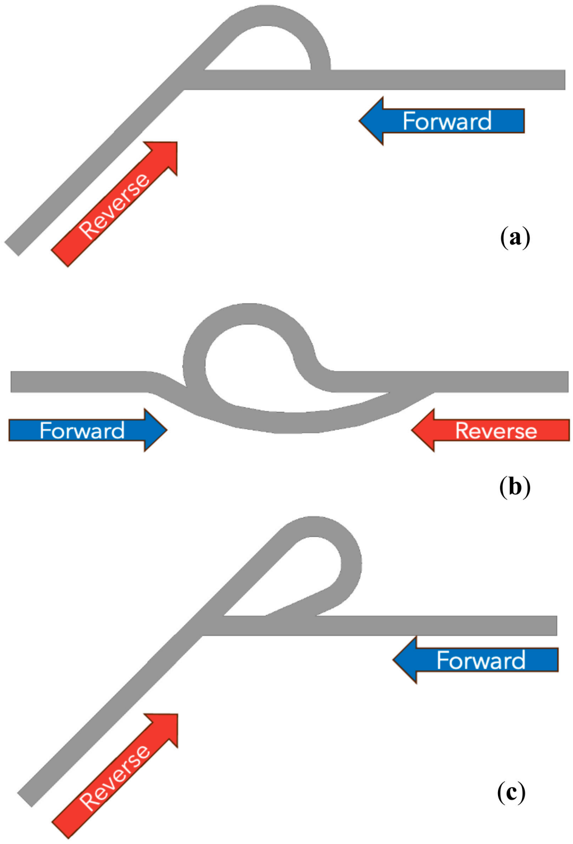

Figure 2. Three types of Tesla valves investigated in this paper: (**a**) T45-R; (**b**) D-valve; (**c**) GMF valve. The forward and reverse directions for each valve are indicated in blue and red arrows. Detailed CAD parameters are adopted from Thompson et al. [11] for the T45-R and GMF valves, and de Vries et al. [7] for the D-valve.

Based on this brief survey, we conjecture that the diodic behavior may remain even if the bifurcated section is removed from a conventional Tesla valve. In this case, the bifurcated branches are replaced by a single bloated middle section. With this kind of geometry, adverse pressure gradients commonly occur as the injected flow enters the bloated section from the narrow inlet. Boundary layer separation and generation of vortices would ensue. While this could occur for the flow in both forward and reverse directions, the system can exhibit a diodic behavior if the adverse pressure gradients and associated effects are more prominent in the reverse direction. Guided by this insight, this study will focus on using CFD simulations to quantify the diodicity associated with the modified Tesla valves without the bifurcated section. The results will be compared to their counterparts of the conventional Tesla valves with bifurcation.

2. Setup of Numerical Experiments

The CFD simulations are performed using Ansys Fluent Version 2023 R2 (ansys.com), a Navier–Stokes equation solver based on the finite volume method. It is equipped with built-in CAD and meshing tools and options of turbulence models. Six configurations of geometry are considered. The bifurcated T45-R valve, D-valve, and GMF valve, as shown in Figure 2, are based on the design parameters given in previous works, the T45-R valve from Figure 3 in Thompson et al. [11], the D-valve from Figure 2 and Table 1 in de Vries et al. [7], and the GMF valve from Figure 6 in Thompson et al. [11]. The counterparts of these three valves without the bifurcated section are created by removing the "island" between the two branches in the geometry. The actual valves used have the width of the inlet (and outlet) set to 0.1 mm in the 2D x–y plane, and 1 mm extrusion in the z direction to form the 3D geometry for CFD simulations. The mesh for the numerical simulation is generated using the built-in meshing tools in Ansys, with a typical element size of approximately 0.01 mm. Regular wall boundary conditions are used on the top and bottom surfaces in the z direction. Although the 3D setting is computationally more costly (approximately 100 grid points are placed in the z direction), we choose it because Thompson et al. [11] have noted that the diodicity produced by 3D simulations matches more closely with experiments, compared to pure 2D simulations. Additionally, Thompson et al. [11] and de Vries et al. [7] have shown that pure 2D simulations tend to overestimate diodicity, particularly at high *Re*. The geometry of our bifurcated T45-R valve follows the same design for the 3D simulations in Thompson et al. [11], which allows us to validate selected results with that paper at low *Re*.

The Ansys Fluent simulations use liquid water with constant density and viscosity. For each configuration of geometry, two sets of "forward" and "reverse" runs are performed by swapping inlet and outlet. Each set consists of 11 runs with a varying Reynolds number (by varying the inlet velocity), *Re* = (50, 100, 150, 200, 250, 300, 500, 800, 1100, 1500, 2000). Here, $Re = \rho UL/\mu$, where ρ is density, μ is dynamic viscosity, U is the imposed inlet velocity, and L is taken as the width of the inlet in the 2D cross section. The results from each pair of forward and reverse runs with the same *Re* are used to compute the diodicity for that case. The turbulence k-ε model in Fluent is turned on, although we do not expect strong turbulence within the chosen range of the Reynolds number. For each case, we seek the steady solution by the iterative process in Ansys Fluent, using the convergence criterion that all scaled residuals reach 10^{-6}.

To assess mesh-independence of the results, extra runs are performed with the same geometry and *Re* but varying mesh resolution. Table 1 shows the forward and reverse pressure drop, and diodicity, from the case of the T45-R valve at *Re* = 300. Five pairs of forward and reverse runs are performed, with the mesh element count increasing from 100 K to 500 K. The setting is comparable to a similar test in Thompson et al. [11]. It is found that, within the range of mesh resolution tested, diodicity fluctuates within 1% of its mean value.

Table 1. Dependence of the pressure drops and diodicity on mesh resolution.

Mesh Element Count	ΔP_r (Pa)	ΔP_f (Pa)	Diodicity
100 K	19,517	15,767	1.238
200 K	19,600	15,866	1.235
300 K	19,681	15,935	1.235
400 K	19,628	15,950	1.231
500 K	19,724	15,953	1.236

3. Results

3.1. T45-R Valve

The T45-R valve is the most basic design of the three valves tested. From CFD simulations, the diodicity of the valve is determined over the range of *Re* = 50–2000. To visualize the flow field, Figure 3 shows the contour plots of velocity magnitude for the simulations at *Re* = 300. Figure 3a,b are the forward and reverse runs for the valve with the bifurcated section. Figure 3c,d are the counterparts of Figure 3a,b for the valve with the island removed. For the forward runs (Figure 3a,c), the main stream of the flow follows two straight paths that connect inlet to outlet with little diversion into the curved path. This is so with or without the bifurcated geometry. For both of the reverse runs (Figure 3b,d), the main stream is diverted into the curved path. Even without the island, the fluid jet in Figure 3d exhibits a strong meander as it enters the bloated section. Thus, the flow in the valve without bifurcation preserves many characteristics of its counterpart in the original valve with bifurcation.

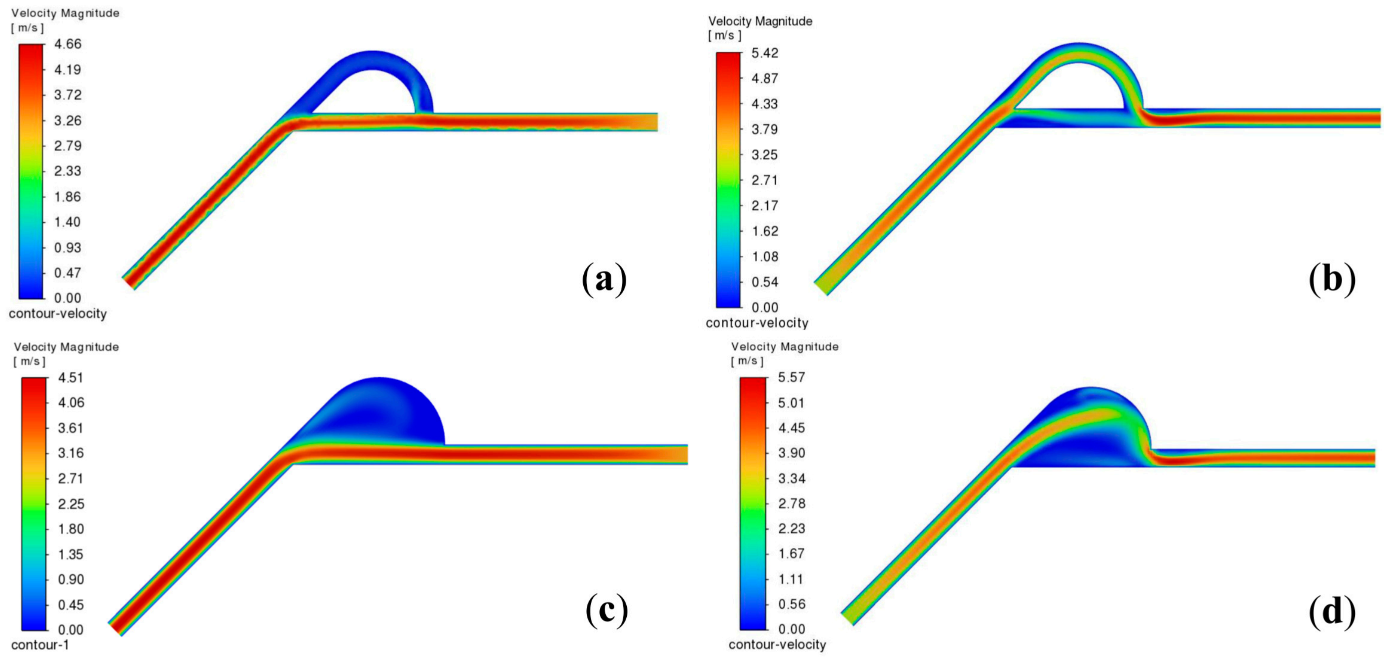

Figure 3. Contour plots of velocity magnitude on the central cross-section for the simulations of the T45-R valve at Re = 300. (**a**) Forward run for the bifurcated version. (**b**) Reverse run for the bifurcated version. (**c**) Forward run for the non-bifurcated version. (**d**) Reverse run for the non-bifurcated version.

The four sets of runs, as shown in Figure 3, are repeated for 11 values of the Reynolds number (detailed in Section 2). The values of diodicity computed from those runs are summarized in Figure 4. For the valve with the bifurcated section (blue in Figure 4), diodicity increases approximately linearly over the range of Re = 50–300, consistent with previous results (e.g., Thompson et al. [11]). At higher values of Re, diodicity continues to increase but only sub-linearly, reaching Di = 1.49 at Re = 2000. Qualitatively, a similar behavior is found for the valve without the bifurcated geometry (red in Figure 4), a linear increase with the Reynolds number up to Re = 250, followed by a sub-linear increase up to Re = 2000 where diodicity reaches Di = 1.66. Interestingly, with an exception at an isolated point (Re = 500), the diodicity for the valve without bifurcation consistently rises above its counterpart for the valve with bifurcation. Thus, we establish an example in which the bifurcated geometry is not absolutely essential for elevating the diodicity of the Tesla valve.

Why is the non-bifurcated case able to achieve a higher value of diodicity? In general, boundary layer separation and generation of vortices occur in the reverse run for both the bifurcated and non-bifurcated cases. While the size of the vortices is limited by the width of the pipe in the bifurcated case, the non-bifurcated valve has more space in the bloated section to permit formation of larger vortices, which are potentially associated with a greater degree of energy dissipation (thus, a greater ΔP_r compared to the bifurcated case). At the same time, the "forward runs" are similar between the bifurcated and non-bifurcated cases; both are characterized by simple straight jets without meanders. It is therefore possible for $\Delta P_r / \Delta P_f$ to be higher for the non-bifurcated case.

While a turbulence model was turned on for our simulations, from the results, the influence of turbulence is not strong over the range of the Reynoleds number considered. Figure 5a shows the contour plot of velocity magnitude at Re = 2000 for the non-bifurcated T45-R valve. The flow structure is similar to the case at Re = 300 (Figure 3d). In other words, a regime transition does not occur between Re = 300 and 2000. Figure 5b shows the turbulent kinetic energy (TKE) from the same run with Re = 2000. Estimated by the square root of TKE, the magnitude of the "perturbation" turbulent velocity is still significantly smaller than the mean velocity for this case.

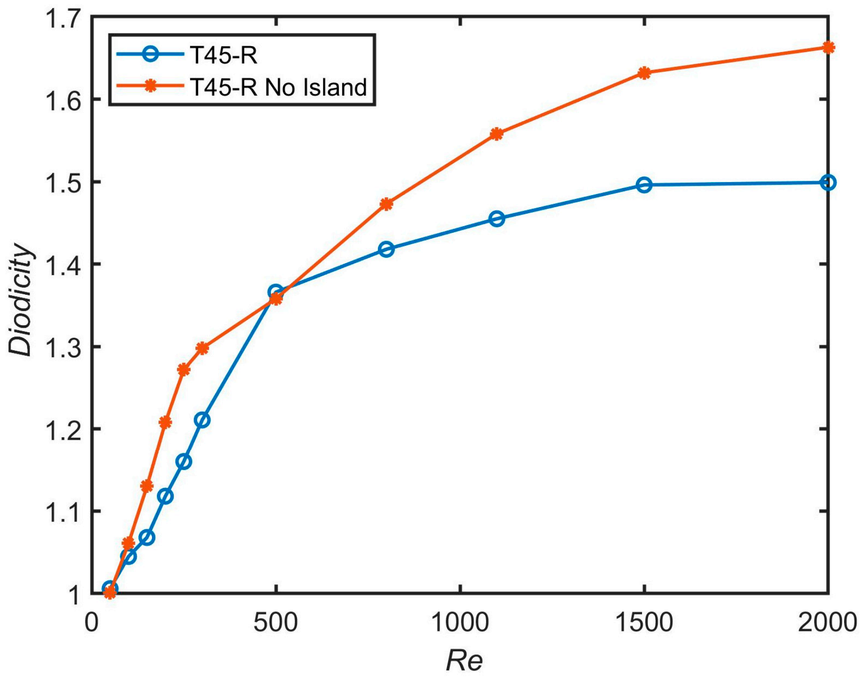

Figure 4. Diodicity as a function of the Reynolds number for the T45-R valve with (blue) and without (red) the bifurcated section.

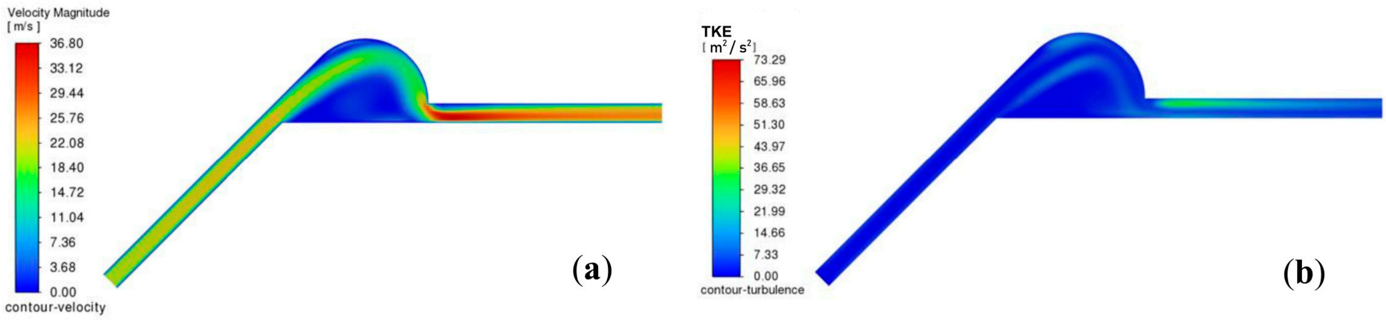

Figure 5. (**a**) Velocity magnitude (in m/s) for the non-bifurcated T45-R valve at *Re* = 2000. (**b**) Turbulent kinetic energy (in m^2/s^2) from the same run.

3.2. D-Valve

The D-Valve is the most complex design of the three valves tested; both branches of its bifurcated section are curved. A non-bifurcated version is created by removing the island between the branches. A series of CFD simulations is performed for *Re* = 50–2000. Figure 6, arranged in the same fashion as Figure 3, shows examples of the flow velocity for the runs at *Re* = 300. The "forward runs" (Figure 6a,c) are very similar between the bifurcated and non-bifurcated cases. Both are characterized by a single jet with minimal branching or meandering. Dramatic differences are found in the "reverse runs" (Figure 6b,d). The bifurcated case exhibits very significant branching, while the non-bifurcated case retains a single jet with little meandering. This is in sharp contrast to the behavior of the T45-R valve (Figure 3b,d) at the same Reynolds number. With the structureless straight jet in Figure 6d, the difference between the reverse and forward runs is minor, and we expect a low diodicity for the non-bifurcated case.

The set of the four runs in Figure 6 is repeated for 11 values of *Re*, with the key result of diodicity vs. *Re* summarized in Figure 7. Indeed, as anticipated from Figure 6, at a low Reynolds number, the diodicity of the non-bifurcated case is far below the bifurcated case. For the bifurcated D-valve, diodicity increases linearly with the Reynolds number up to *Re* = 300. Above it, diodicity continues to increase, but only sub-linearly, attaining *Di* = 1.94

at *Re* = 2000. This exceeds the value for the T45-R valve with or without bifurcation. For the non-bifurcated valve, diodicity remains low (but gradually increasing with *Re*) until passing *Re* = 1100, then increases significantly to reach *Di* = 2.00 (slightly exceeding its counterpart for the bifurcated valve) at *Re* = 2000.

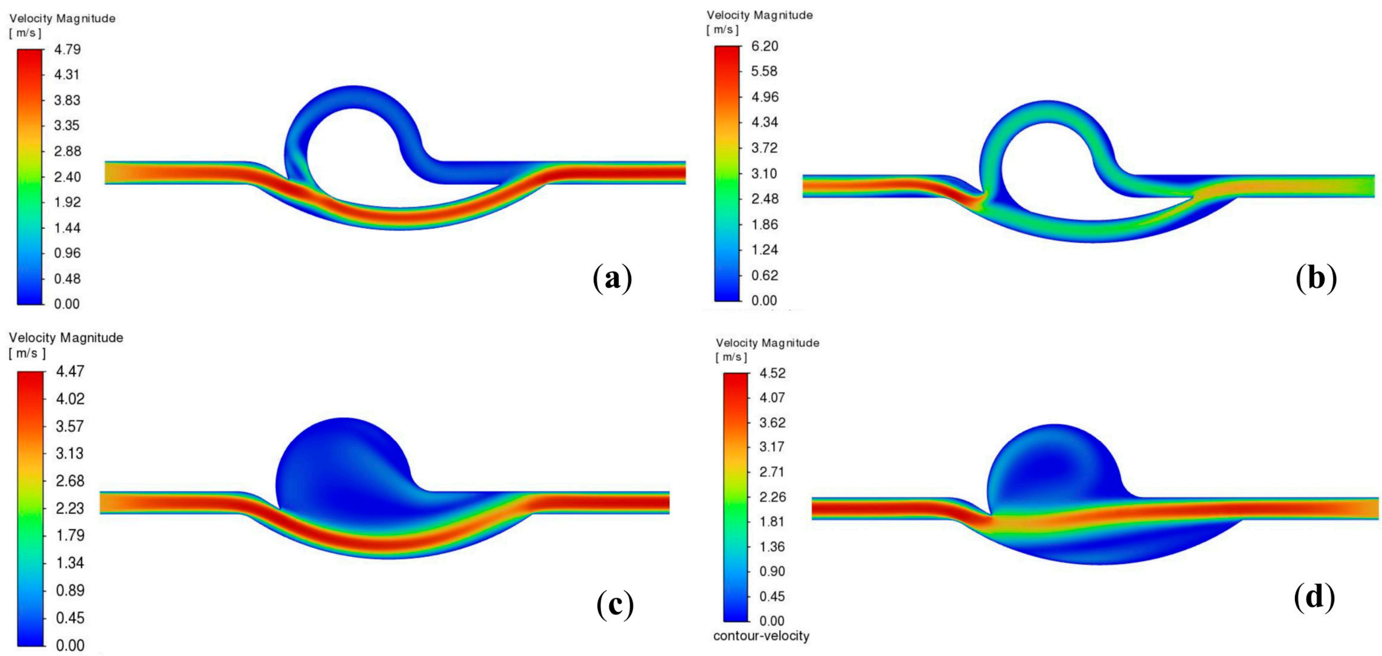

Figure 6. Contour plots of velocity magnitude for the simulations of the D-valve at *Re* = 300. (**a**) Forward run for the bifurcated version. (**b**) Reverse run for the bifurcated version. (**c**) Forward run for the non-bifurcated version. (**d**) Reverse run for the non-bifurcated version.

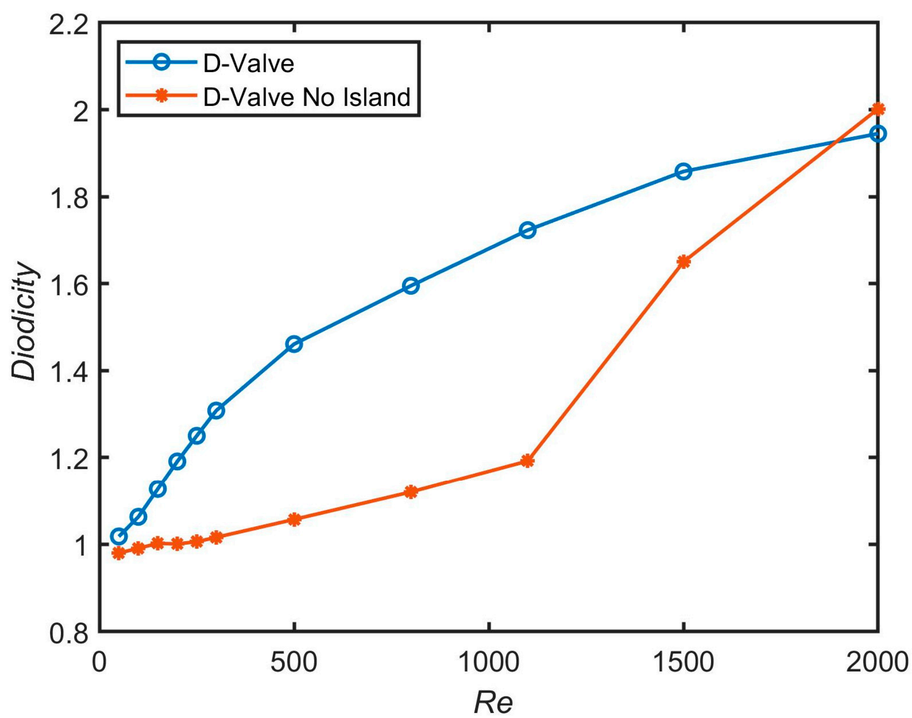

Figure 7. Diodicity as a function of the Reynolds number for the D-valve with (blue) and without (red) the bifurcated section.

The low diodicity for the non-bifurcated case at low *Re* is likely due to the D-Valve lacking an incoming angled flow characteristic such as on the T45-R and GMF valves. The flow is horizontal for the D-valve, and without a bifurcated section, the low-speed flow moves with minimal resistance across the valve in the reverse and forward directions. This "straight jet" state would not remain stable at high Reynolds numbers. Eventually, a transition to a state of branching or meandering jet would occur at a sufficiently high *Re*. This leads to an enhanced level of energy dissipation, which we conjecture is related to the significant uptick of diodicity for the non-bifurcated valve when the Reynolds number passes 1100.

While the behavior of the D-valve is somewhat complicated at higher Reynolds numbers, for $Re \leq 1100$ we establish a clear example in which the bifurcated section is essential for elevating the diodicity of the Tesla valve.

3.3. GMF Valve

The GMF valve was previously known to achieve a higher diodicity compared to the T45-R and D-valve over the range of $Re \leq 600$ (de Vries et al. [7], based on 2D simulations). It can be thought of as a variation of the T45-R design but with an acute angle at the junction where the curved branch rejoins the straight segment of the pipe. A non-bifurcated version of the valve is created, and CFD simulations are performed for both versions for *Re* = 50–2000. Figure 8 shows the velocity magnitude for the simulations at *Re* = 300. The behavior of the forward runs (Figure 8a,c) is similar to the case for the T45-R valve (Figure 3a,c). The fluid jet sticks to a nearly straight path without meandering or branching. The reverse run for the bifurcated GMF valve also behaves like the T45-R case, with the main stream diverted into the curved section. In contrast, in the reverse run for the non-bifurcated valve, the fluid jet stays close to the straight path instead of significantly meandering like the T45-R case. The small difference between forward and reverse runs for the non-bifurcated valve would imply a low diodicity.

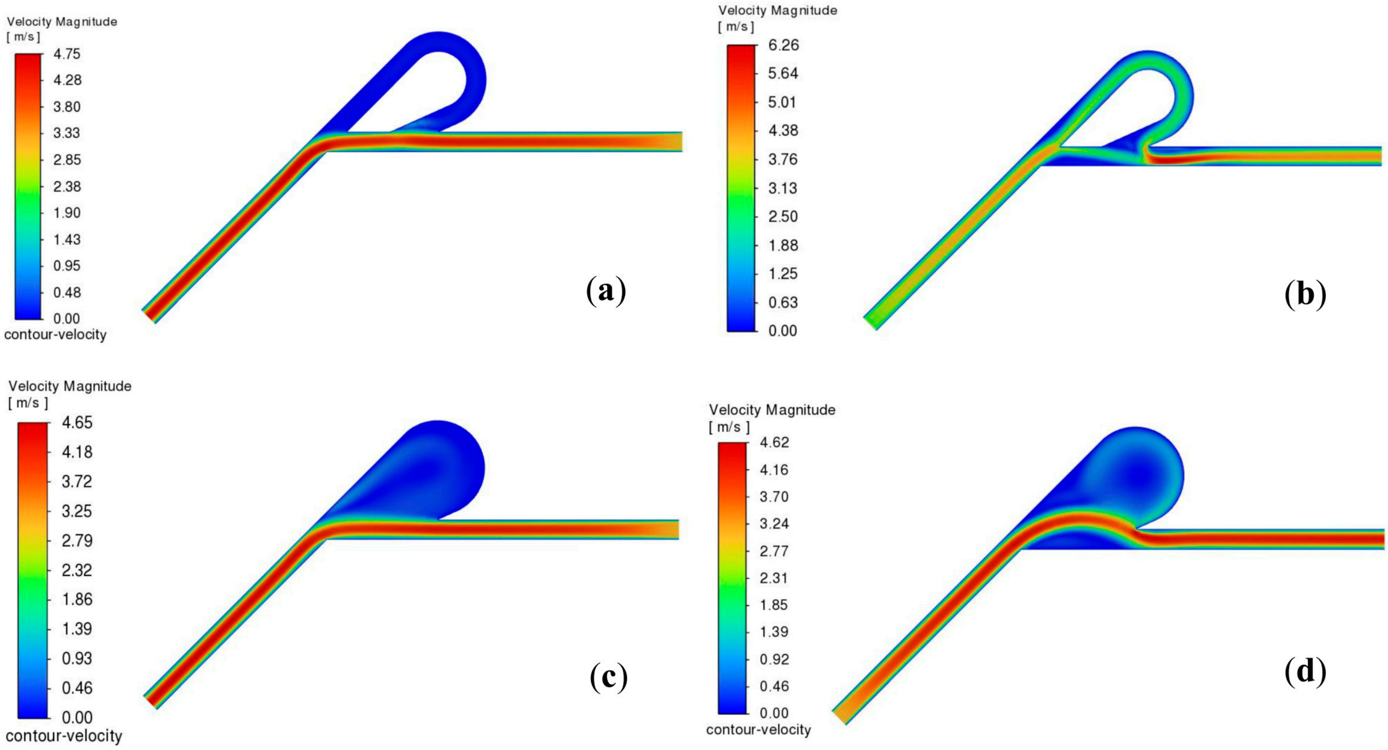

Figure 8. Contour plots of velocity magnitude for the simulations of the GMF valve at *Re* = 300. (**a**) Forward run for the bifurcated version. (**b**) Reverse run for the bifurcated version. (**c**) Forward run for the non-bifurcated version. (**d**) Reverse run for the non-bifurcated version.

Figure 9 summarizes diodicity vs. Re from all simulations for the GMF valve. As expected from Figure 8, for the non-bifurcated valve, the diodicity stays low at low Re. It increases slightly up to $Re = 500$ then levels off, reaching only $Di = 1.15$ at $Re = 2000$. A transition of an uptick of diodicity like the case of the non-bifurcated D-valve does not occur. This likely reflects the situation that the near-straight jet structure seen at a low Reynolds number does not transition to a strongly meandering or branching state even when Re is increased to 2000. The result for the bifurcated GMF valve is also interesting. Previous studies have shown that the diodicity for this case increases linearly with the Reynolds number for $Re < 500$, then levels off over $Re = 500$–600 (de Vries et al. [6], but note that the relevant result therein was based on 2D simulations which tend to overestimate diodicity). Qualitatively, this behavior is recovered in Figure 9. For $Re \geq 800$, we find that diodicity begins to decrease with Re, reaching $Di = 1.35$ at $Re = 2000$ (compared to the peak value of $Di = 1.82$ at $Re = 800$). The reason for this declining trend remains to be investigated. We conjecture that, at a high Reynolds number, structures such as vortices also begin to emerge in the forward run. The ratio of $\Delta P_r / \Delta P_f$ would decline if the increase in ΔP_f overcompensates that in ΔP_r.

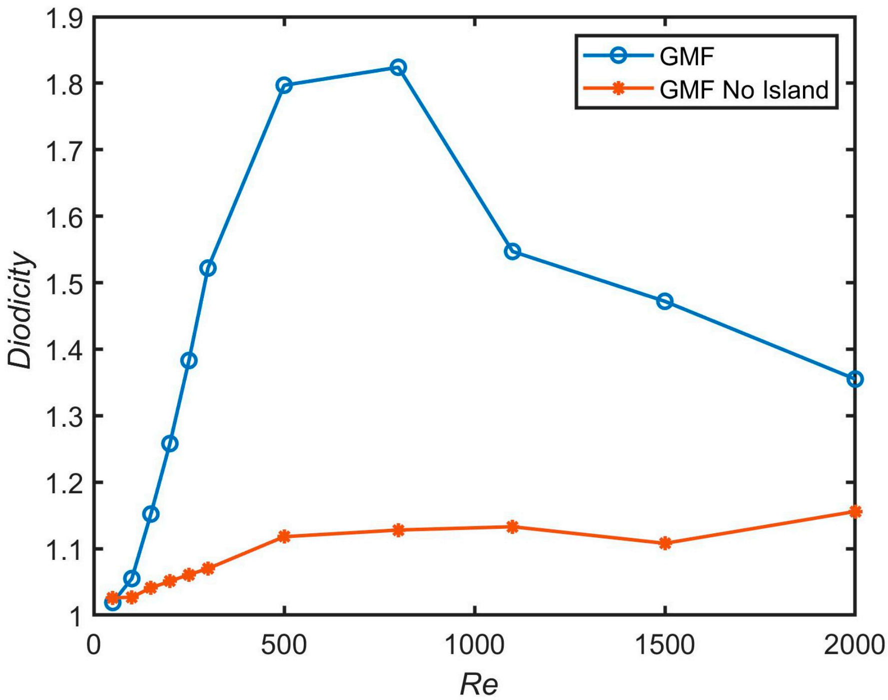

Figure 9. Diodicity as a function of the Reynolds number for the GMF valve with (blue) and without (red) the bifurcated section.

For the GMF valve over the range of $Re \leq 2000$, we establish another clear case in which the bifurcated geometry is essential for sustaining a high level of diodicity.

4. Discussion

The three cases we investigated exhibit diverse behaviors for the dependence of diodicity on the bifurcated geometry, and on the Reynolds number. In the reverse run, the bifurcated geometry of a Tesla valve forces the flow from inlet to always branch into a curved path. When the island between the branches is removed, the injected flow may remain nearly straight as it enters the bloated mid-section. This happens for the D-valve for $Re \leq 1100$ and the GMF valve over a wider range of Re. For these two cases, the lack of energy-dissipating structures in the reverse run results in a low diodicity. These are the cases in which the bifurcated design is essential for sustaining a high diodicity. An uptick of diodicity occurs for the non-bifurcated D-valve when $Re > 1100$. We conjecture that this is due to a transition from a straight jet at a low Reynolds number to a branched or meandering jet at a higher Reynolds number in the reverse run. Such a transition has likely not occurred for the GMF valve up to $Re = 2000$. In future work, it will be interesting to test the behavior of the GMF valve at higher Reynolds numbers, and to pinpoint the Reynolds number for the transition for both the non-bifurcated D-valve and GMF valve.

In contrast to the cases of the D-valve and GMF valve, in the reverse run of the non-bifurcated T45-R valve, a meandering jet is already established in the bloated section, even at relatively low Re. As a result, through the range of the Reynolds number tested, the diodicity of the non-bifurcated valve is comparable to, and even rises above, its counterpart of the bifurcated design. Nevertheless, for practical applications, the diodicity of the non-bifurcated T45-R valve still falls below that of the bifurcated D-valve for $Re \leq 2000$ and GMF valve for $Re \leq 800$.

Although an increased diodicity with the removal of the island is found only for T45-R, more such examples might exist among other variations of Tesla valves. An expanded search could first test the variations of the three valves used in this study. For example, the angle between the inlet and outlet can be altered for the T45-R and GMF valves to form new variations. Analyzing the results from a larger collection of valves may help sharpen our understanding of the relation between valve geometry and diodicity.

The estimates of diodicity in this study are based solely on numerical simulations. Experimental data on diodicity is far from abundant and available only at low Reynolds numbers. Thompson et al. [11] compared their 3D numerical results for the bifurcated T45-R valve with the experimental data from Forster et al. [10] and found a close agreement at $Re = 200$–250. Since we adopted a similar setting to Thompson et al. [11] and validated our numerical results with theirs at these Reynolds numbers, this also indirectly validates our results with the experiments in Forster et al. [10]. However, these few data points only cover a small portion of the cases we simulated. For $Re > 300$, and generally for the D-valve and GMF valve, we hope future work will bridge the gap in experimental validation.

Another useful future work is to test the dependence of the numerical results on the CFD model at higher Reynolds numbers. As we need to perform a large number of 3D simulations across a wide range of Reynolds numbers up to $Re = 2000$, in this study we chose to use a relatively modest resolution and invoke a turbulence k-ε model, letting it treat sub-gridscale effects at higher Reynolds numbers (in our setting, turbulence is not overwhelming but does have some effects at $Re = 2000$, as shown in Figure 5). This choice is computationally less costly compared to DNS, but at the expense of uncertainties in the turbulence model. In future testing, contrasting runs could be performed by altering the parameters in the model or replacing it with a different type (e.g., k-Ω) of turbulence model. More generally, in the range of small to intermediate Reynolds numbers, one may choose to use a laminar model (and increase the resolution sufficiently to achieve DNS) and compare the result. At higher Reynolds numbers (e.g., Re = 1000–2000), the laminar-DNS model might produce a transient solution. Analyzing such cases would be of its own independent interest.

The preceding discussions point to useful future directions of CFD analysis on other new designs of Tesla valves and at higher Reynolds numbers. It will also be useful to expand the current study to the multi-staged setting, for multiple Tesla valves in a chain.

5. Conclusions

In this study, we investigated the effects of removing the bifurcated section from Tesla-type valve designs on their efficiency, quantified by diodicity, over the range of $Re = 50$–2000. From 3D CFD simulations, diodicity is quantified for three distinct designs: T45-R, D-valve, and GMF valve, with and without the bifurcated section. For the T45-R valve, removing the bifurcated section actually leads to a consistent increase in diodicity, particularly at high Re. In contrast, the diodicity of the GMF valve drops significantly when the bifurcated section is removed. The behavior of the D-valve is in-between those two cases. Its non-bifurcated version exhibits a suppressed diodicity at low Reynolds numbers, but an uptick of diodicity after *Re* passes 1100 such that the non-bifurcated and bifurcated valves have about the same diodicity at *Re* = 2000.

We interpret the results by considering the structure of the injected jet in the bloated section in the reverse run for the non-bifurcated valve. In general, at low *Re*, the jet may remain nearly straight and structureless. With an increasing *Re*, a transition occurs, which gives rise to a branched or meandering jet. The emerging structures lead to a greater energy dissipation for the reverse run, and thereby a greater diodicity. For the T45-R valve, the state of a meandering jet is reached at very low *Re*. We conjecture that for the D-valve, the transition occurs at *Re* ~ 1100, while for the GMF valve it does not occur for *Re* up to 2000. This will hopefully motivate future work to search for the transition for different designs of Tesla valves at higher Reynolds numbers.

The 3D CFD simulations are also used to quantify the diodicity of the bifurcated valves over previously unexplored ranges of *Re*. For *Re* = 500–2000, a sub-linear increase of diodicity with *Re* is found for the T45-R and D-valve. In contrast, for the GMF valve, the diodicity peaks at *Re* ~ 800, then begins to decrease with *Re*. Thus, even within the classical bifurcated designs, non-trivial behaviors exist for the dependence of diodicity on the Reynolds number.

Overall, this study highlights the crucial role of valve geometry, particularly the presence or absence of the bifurcated section, in influencing diodicity. Our conclusions have implications for future designs of Tesla-type valves and their applications in flow control and optimization.

Author Contributions: Conceptualization, S.W. and H.-P.H.; methodology, S.W and H.-P.H.; software, S.W.; validation, S.W.; formal analysis, S.W.; investigation, S.W. and H.-P.H.; writing—original draft preparation, S.W.; writing—review and editing, S.W. and H.-P.H. All authors have read and agreed to the published version of the manuscript.

Funding: This research received no external funding.

Data Availability Statement: All results are based on computer simulation. The settings of key parameters for the simulations are available from the authors.

Acknowledgments: This paper is based in part on the honors thesis of the first author, completed at Arizona State University. The authors thank two anonymous reviewers for their useful comments.

Conflicts of Interest: The authors declare no conflicts of interest.

References

1. Tesla, N. Valvular Conduit. U.S. Patent Number 1329559, 3 February 1920.
2. Begg, R. The Tesla Valve: Bringing Back a Forgotten Invention, Machine Design. 2023. Available online: https://www.machinedesign.com/mechanical-motion-systems/article/21164409/the-tesla-valve-bringing-back-a-forgotten-invention (accessed on 1 November 2024).
3. Li, W.; Yang, S.; Chen, Y.; Li, C.; Wang, Z. Tesla valves and capillary structures-activated thermal regulator. *Nat. Commun.* **2023**, *14*, 3996. [CrossRef] [PubMed]
4. Raffel, J.; Ansari, S.; Nobes, D.S. An experimental investigation of flow phenomena in a multistage micro-Tesla valve. *J. Fluid Eng.* **2021**, *143*, 111205. [CrossRef]
5. Wang, J.; Cui, B.; Liu, H.; Chen, X.; Li, Y.; Wang, R.; Lang, T.; Yang, H.; Li, L.; Pan, H.; et al. Tesla valve-based flexible microhybrid chip with unidirectional flow Properties. *ACS Omega* **2022**, *7*, 31744–31755. [CrossRef] [PubMed]
6. Zhang, S.; Winoto, S.H.; Low, H.T. Performance simulations of Tesla Microfluidic Valves. In Proceedings of the International Conference on Integration and Commercialization of Micro and Nanosystems, Sanya, China, 10–13 January 2007; pp. 15–19.
7. de Vries, S.F.; Florea, D.; Homburg, F.G.A.; Frijns, A.J.H. Design and operation of a Tesla-type valve for pulsating heat pipes. *Int. J. Heat Mass Transf.* **2017**, *105*, 1–11. [CrossRef]
8. Monika, K.; Chakraborty, C.; Roy, S.; Sujith, R.; Datta, S.P. A numerical analysis on multi-stage Tesla valve based cold plate for cooling of pouch type Li-ion batteries. *Int. J. Heat Mass Transf.* **2021**, *177*, 121560. [CrossRef]
9. Gajjar, K.; Huang, H.-P. Conjugate heat transfer for single phase immersion cooling of CPU. *Case Stud. Therm. Eng.* **2023**, *52*, 103728. [CrossRef]
10. Forster, F.K.; Bardell, R.L.; Afromowitz, M.A.; Sharma, N.R.; Blanchard, A. Design, Fabrication and Testing of Fixed-Valve Micro-Pumps. *Asme-Publications-Fed* **1995**, *234*, 39–44.

11. Thompson, S.M.; Paudel, B.J.; Jamal, T.; Walters, D.K. Numerical investigation of multistaged Tesla Valves. *J. Fluids Eng.* **2014**, *136*, 081102. [CrossRef]
12. Gamboa, A.R.; Morris, C.J.; Forster, F.K. Improvements in Fixed-Valve Micropump Performance Through Shape Optimization of Valves. *ASME J. Fluid Eng.* **2005**, *127*, 339–346. [CrossRef]
13. Wang, C.-T.; Chen, Y.-M.; Hong, P.-A.; Wang, Y.-T. Tesla valves in micromixers. *Int. J. Chem. React. Eng.* **2014**, *12*, 397–403. [CrossRef]
14. Pattanshetti, A. Tesla Valve: How Does It Work? Published on 26 September 2022. Available online: https://www.lesics.com/how-tesla-valve-works.html (accessed on 1 November 2024).
15. Zeidan, M.; Németh, M.; Abhijith, G.R.; Wéber, R.; Ostfeld, A. Transient flow dynamics in Tesla valve configurations: Insight from computational fluid dynamics simulations. *Water* **2024**, *16*, 3492. [CrossRef]